

# Stability of the monoclinic phase in the ferroelectric perovskite $\text{PbZr}_{1-x}\text{Ti}_x\text{O}_3$ .

B. Noheda \*, D.E. Cox and G. Shirane.

*Physics Department, Brookhaven National Laboratory, Upton, NY 11973*

R. Guo, B. Jones and L.E. Cross

*Materials Research Laboratory, The Pennsylvania State University, University Park, PA 16802*

Recent structural studies of ferroelectric  $\text{PbZr}_{1-x}\text{Ti}_x\text{O}_3$  (PZT) with  $x = 0.48$ , have revealed a new monoclinic phase in the vicinity of the morphotropic phase boundary (MPB), previously regarded as the the boundary separating the rhombohedral and tetragonal regions of the PZT phase diagram. In the present paper, the stability region of all three phases has been established from high resolution synchrotron x-ray powder diffraction measurements on a series of highly homogeneous samples with  $0.42 \leq x \leq 0.52$ . At 20K the monoclinic phase is stable in the range  $0.46 \leq x \leq 0.51$ , and this range narrows as the temperature is increased. A first-order phase transition from tetragonal to rhombohedral symmetry is observed only for  $x = 0.45$ . The MPB, therefore, corresponds not to the tetragonal-rhombohedral phase boundary, but instead to the boundary between the tetragonal and *monoclinic* phases for  $0.46 \leq x \leq 0.51$ . This result provides important insight into the close relationship between the monoclinic phase and the striking piezoelectric properties of PZT; in particular, investigations of poled samples have shown that the monoclinic distortion is the origin of the unusually high piezoelectric response of PZT.

## I. INTRODUCTION

Exceptionally striking dielectric and piezoelectric properties are found in  $\text{PbZr}_{1-x}\text{Ti}_x\text{O}_3$  (PZT), the perovskite-type oxide system which is the basis of practically all transducers and other piezoelectric devices. This solid solution is cubic at high temperatures but becomes slightly distorted at lower temperatures, where it is ferroelectric. Except for a narrow region close to  $\text{PbZrO}_3$ , the ferroelectric phase is divided in two regions of different symmetry, rhombohedral for Zr-rich compositions and tetragonal for Ti-rich compositions. The highest piezoelectric response in this system is found at the nearly vertical boundary between these two phases, at  $x \simeq 0.47$ ; the so-called morphotropic phase boundary (MPB), as defined by Jaffe *et al.* [1]. The PZT phase diagram for compositions around the MPB is shown in Fig.1, where the open circles represent the data of Jaffe *et al.* [1], which define the MPB above room temperature. The sharpness of this line is such that a composition fluctuation of  $\Delta x = 0.01$  corresponds to a temperature uncertainty of  $\Delta T \simeq 90$  K. Recently, high resolution x-ray diffraction measurements on extremely homogenous samples by Noheda *et al.* showed that an intermediate monoclinic phase exists between the rhombohedral and tetragonal PZT phases [2-4]. The observation of this monoclinic phase in two different compositions,  $x = 0.48$  [2,4] and  $x = 0.50$  [3], has allowed a preliminary modification of the phase diagram, as shown in Fig. 1. Furthermore, the discovery of this phase around the MPB in PZT answers many of the questions raised by previous investigators [5-10] about the

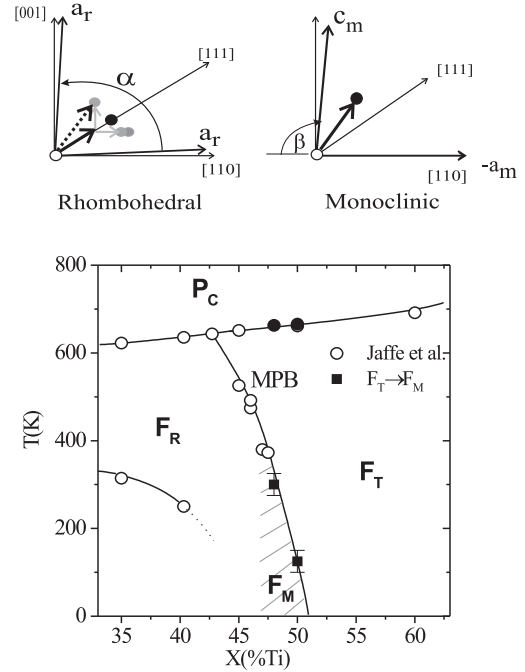


FIG. 1. The lower part of the figure shows the PZT phase diagram close to the MPB reported by Jaffe *et al.* [1] (open symbols), and the preliminary modification proposed in ref. 3, including the monoclinic phase. The solid symbols represent the observed phase transitions for  $x = 0.48$  [4] and  $x = 0.50$  [3]. The upper part of the figure depicts the microscopic model proposed for the rhombohedral and the monoclinic phases in ref. [4] (see text).

nature of the MPB and the underlying basis for the special physical properties of PZT in this region of the

phase diagram, especially in the context of the coexistence of rhombohedral and tetragonal phases.

The monoclinic unit cell is doubled with respect to the tetragonal one and has  $b$  as the unique axis.  $a_m$  and  $b_m$  are directed along the pseudo-cubic  $[1\bar{1}0]$  and  $[1\bar{1}0]$  directions, respectively, while  $c_m$  is close to the tetragonal  $c$  axis, along  $[001]$ , but tilted away from it such that the angle,  $\beta$ , between  $a_m$  and  $c_m$  is slightly larger than  $90^\circ$ . This monoclinic phase has unique characteristics in comparison to all other ferroelectric perovskite phases. The polar axis is not determined by symmetry and can be directed anywhere within the monoclinic  $ac$  plane; that is, the polar axis is allowed to rotate within this plane. In the case of PZT, the pseudo-cubic  $[111]$  and  $[001]$  directions are contained within the monoclinic plane and the monoclinic polar axis is tilted away from the polar axis of the tetragonal phase,  $[001]$ , towards that of the rhombohedral phase,  $[111]$  [4]. As has already been pointed out by other authors [11–13], the diffraction data show clearly that the local structure of PZT differs from that of the average one. A structure analysis of rhombohedral PZT by Corker et al. [13] indicated that the Zr/Ti cations in the Zr-rich compositions are distributed among three locally-disordered sites with monoclinic symmetry (see the gray circles in the top-left plot of Fig. 1), resulting in average rhombohedral symmetry (black circle in the top-left plot of Fig. 1.) [4]. In a similar structure analysis of tetragonal PZT close to the MPB [4], the diffraction data were shown to be consistent with Zr/Ti cations distributed among four locally-disordered cation sites with monoclinic symmetry, resulting in average tetragonal symmetry [4].

In recent years, the development of first-principles calculations applied to the study of ferroelectric perovskites has contributed greatly to the understanding of the physical properties of these materials (see, e.g., refs. [14–19]). The incorporation of a compositional degree of freedom to allow for the study of solid solutions has been an important advance which has opened up the possibility of investigating more complex ferroelectric materials such as PZT and related systems [20–26]. Very recently, Bellaiche *et al.* [27] have succeeded to derive the monoclinic phase of PZT from first-principles calculations. These authors also show that the value of the piezoelectric coefficient calculated taking into account rotation of the polarization vector in the monoclinic plane is in good agreement with the high values observed in PZT.

In the present work, the stability region of the monoclinic phase in PZT is characterized by means of synchrotron x-ray powder diffraction measurements made on PZT compositions at closely-spaced intervals in the range  $x = 0.42$ – $0.52$ . The monoclinic phase is observed at 20K for  $0.46 \leq x \leq 0.51$  and this composition range narrows as the temperature increases. The transition temperature between the tetragonal and monoclinic phases is very steep as a function of composition and coincides with

the previously mentioned MPB of Jaffe *et al.* [1] above ambient temperature.

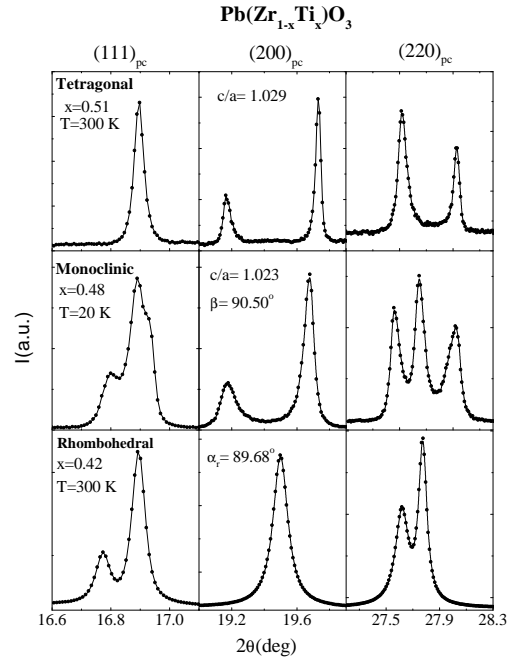


FIG. 2. Pseudo-cubic (111), (200) and (220) reflections for PZT with  $x = 0.51$  at 300K (top),  $x = 0.48$  at 20K (center) and  $x = 0.42$  at 300 K (bottom), showing the distinctive features of the tetragonal, monoclinic and rhombohedral PZT phases, respectively.

## II. EXPERIMENTAL

PZT samples with  $x = 0.42, 0.45, 0.46, 0.47, 0.50, 0.51$  and  $0.52$  were prepared by conventional solid-state reaction techniques similar to those used previously for PZT with  $x = 0.48$  [4]. During the calcination, two steps were used. First, the desired solid solution was formed at  $900^\circ\text{C}$  using the appropriate amounts of reagent-grade powders of lead carbonate, zirconium oxide and titanium oxide with chemical purity better than 99.9 %. Second, the formed product was pulverized and allowed to reach homogeneity by heating for six hours at  $850^\circ\text{C}$  (lower than the temperature at which  $\text{PbO}$  evaporates). Pellets were then pressed using an organic binder and, after burn out of the binder, heated to  $1250^\circ\text{C}$  at a ramp rate of  $10^\circ\text{C}/\text{min}$ , held at this temperature in a covered crucible for 2 hours, and cooled down to room temperature. During sintering,  $\text{PbZrO}_3$  was used as a lead source to maintain a  $\text{PbO}$ -rich atmosphere.

Several sets of high-resolution synchrotron x-ray powder diffraction measurements were made on different oc-

casions at beam line X7A at the Brookhaven National Synchrotron Light Source. Data were collected from the ceramic disks in symmetric flat-plate reflection geometry using  $\theta$ - $2\theta$  scans over selected angular regions in the temperature range 20-750 K. The sample was rocked  $1$ - $2^\circ$  during data collection to improve powder averaging. In all these experiments a Ge(111) double-crystal monochromator was used to provide an incident beam with a wavelength close to  $0.7 \text{ \AA}$ . A Ge(220) crystal analyzer and scintillation detector were mounted in the diffracted beam, giving an instrumental resolution of about  $0.01^\circ$  on the  $2\theta$  scale. As described in ref. [4], measurements above room temperature were performed with the disk mounted inside a wire-wound BN tube furnace. The accuracy of the temperature in the furnace is estimated to be about  $10 \text{ K}$ . For low-temperature measurements, the pellet was loaded in a closed-cycle He cryostat, which has an estimated temperature accuracy of  $2 \text{ K}$ . With this type of diffraction geometry it is not always possible to eliminate preferred orientation and texture effects, but the peak positions, on which the present results are based, are not affected.

In many cases the peak profiles were quite complex, necessitating a very detailed and careful peak-fitting analysis. The peak positions were determined from least-squares fits to the profile recorded for each of the selected regions. A pseudo-Voigt peak shape function with an asymmetry correction was used [28], and factors such as anisotropic peak widths, coexisting phases and diffuse scattering between peaks were taken into account. The lattice parameter of individual phases were obtained from fits to the observed peak positions for several reflections. Because of the complicated peak shapes, we found that the above procedure gave more consistent results than standard profile-fitting programs.

Examples of selected regions of the diffraction patterns for the three PZT phases, tetragonal (top), monoclinic (center) and rhombohedral (bottom), around the morphotropic phase boundary are shown in Figure 2. The narrow width of the peaks demonstrates the excellent quality of the ceramic samples and allows the specific characteristics of each phase to be clearly distinguished. In particular, the monoclinic phase exhibit unique features that cannot be accounted for either of the other phase or a mixture of them. In the monoclinic phase the unit cell is doubled in volume with respect to the tetragonal one, with  $a_m$  and  $b_m$  lying along the tetragonal  $[1\bar{1}0]$  and  $[11\bar{0}]$  directions, and  $c_m$  tilted slightly away from the  $[001]$  direction. The monoclinic phase illustrated in this figure corresponds to the composition  $x=0.48$  at  $20\text{K}$ , described in detail in ref. [4], with  $a_m=5.721 \text{ \AA}$ ,  $b_m=5.708 \text{ \AA}$ ,  $c_m=4.138 \text{ \AA}$  and  $\beta=90.50^\circ$ . The  $c/a$  value in Fig. 2 (center) is defined as  $2\sqrt{2}c_m/(a_m+b_m)$ , in order to correspond to the  $c_t/a_t$  ratio in the tetragonal case (top).

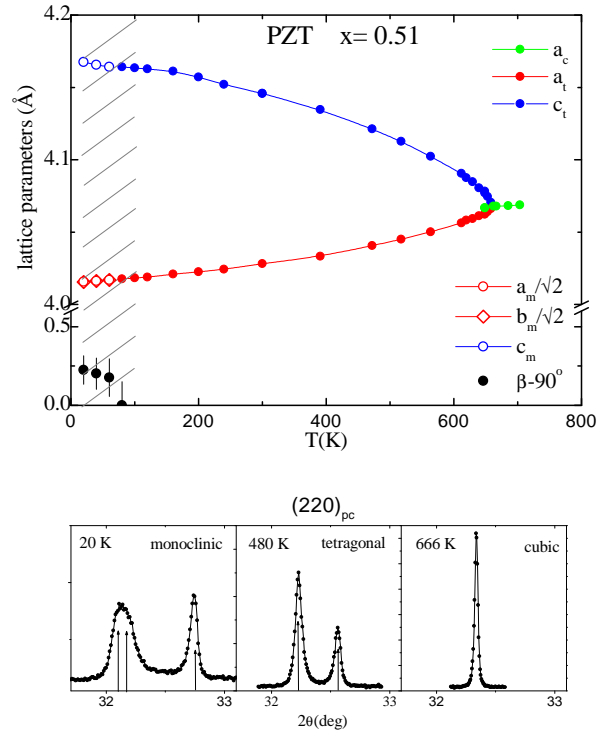


FIG. 3. Temperature evolution of the lattice parameters of PZT with  $x=0.51$  from 20 K to 700 K, for the monoclinic,  $a_m$ ,  $b_m$ ,  $c_m$  and  $\beta$ ; tetragonal,  $a_t$  and  $c_t$ ; and cubic,  $a_c$ , phases. The dashed region in the figure represents the uncertainty in the tetragonal-monoclinic phase transition. At the bottom of the figure the pseudo-cubic (220) reflection is plotted at 20 K (monoclinic), 480 K (tetragonal) and 666 K (cubic), to illustrate the differences between the three phases.

### III. PHASE TRANSITIONS

The evolution of the different structures as a function of temperature has been determined for all the PZT samples in the present study ( $x=0.42, 0.45, 0.46, 0.47, 0.51$  and  $0.52$ ), and combined with previous data obtained for  $x=0.48$  and  $x=0.50$  [2,4]. These results give a complete picture of the phase transitions occurring around the morphotropic phase boundary from 20 to 700K. Three different low temperature phases, with rhombohedral, monoclinic and tetragonal symmetry, are observed. An important result is that the MPB defined by Jaffe *et al.* [1] is shown to correspond to the limit of the *monoclinic* phase rather than that of the rhombohedral phase, and is a very robust line that is reproduced for all the samples under investigation. Both the tetragonal-monoclinic and the tetragonal-rhombohedral phase transitions will be described in this section, as well as the rhombohedral-rhombohedral phase transitions observed for  $x=0.42$  at lower temperatures.

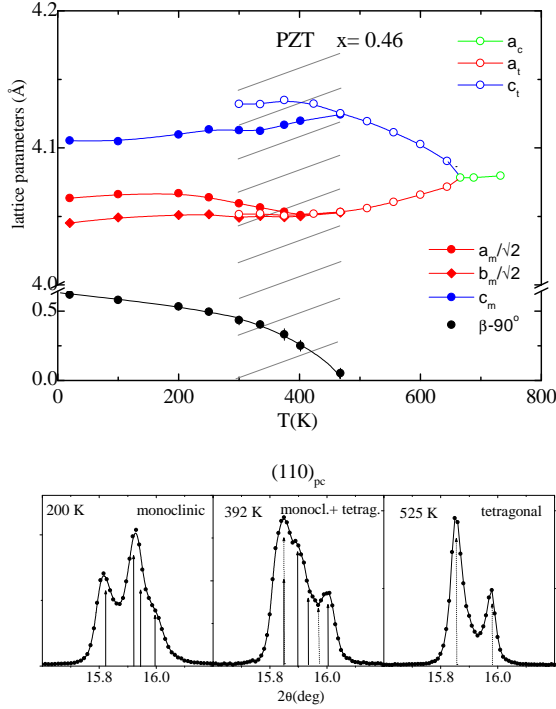


FIG. 4. Temperature evolution of the lattice parameters of PZT with  $x=0.46$  from 20 K to 710 K, for the monoclinic,  $a_m$ ,  $b_m$ ,  $c_m$  and  $\beta$ ; tetragonal,  $a_t$  and  $c_t$ ; and cubic,  $a_c$ , phases. The dashed area in the figure represents the region of tetragonal and monoclinic phase coexistence. At the bottom of the figure the pseudo-cubic (110) reflection is plotted at 200 K (monoclinic phase), 392 K (tetragonal/monoclinic phase coexistence) and 525 K (tetragonal phase), where the calculated peak positions are indicated by solid arrows in the monoclinic phase and dashed arrows in the tetragonal phase.

### A. Tetragonal-monoclinic phase transition

The tetragonal phase in PZT is very similar to that of pure  $\text{PbTiO}_3$  [29–31]. The effects of Zr substitution on the structure of the tetragonal phase are basically two: first, as the Zr content increases, the tetragonal strain,  $c_t/a_t$ , decreases, and, second, the cubic-to-tetragonal phase transition evolves from first-order to second-order. Figure 3 (top) shows the lattice parameters of PZT with  $x=0.51$  as a function of temperature. The paraelectric-ferroelectric phase transition at  $T \simeq 660$  K is of second order, as expected [32], and the ferroelectric phase is purely tetragonal down to 100 K. Below this temperature structural changes can be noticed; in particular, the tetragonal  $(h0h)_t$  and  $(hhh)_t$  reflections broaden markedly. This is apparent in the lower part of Fig. 3, where the pseudo-cubic  $(220)_{pc}$  reflections are shown at high temperature (right), at an intermediate temperature (center), and at low temperature (left). Based on a

careful peak-fitting analysis, the broadening at low temperatures of these reflections can be attributed to two separated peaks, consistent with the monoclinic symmetry observed in PZT with  $x=0.48$  [4], also illustrated in Fig. 2. However, the monoclinic distortion is quite small being  $a_m \simeq b_m$  and  $\beta \simeq 90.2^\circ$ . Similar behavior was observed for a sample of PZT with  $x=0.50$  [3] prepared under slightly different conditions, to be discussed later. As seen from Fig. 3, the monoclinic angle,  $\beta$ , is small and the tetragonal-to-monoclinic transition temperature can only be approximately defined at  $T_{T-M} \simeq 50$  K. On the other hand, data collected from PZT with  $x=0.52$  show a well-defined tetragonal phase down to 20 K.

The evolution of the lattice parameters with temperature for PZT with  $x=0.46$  is shown in Figure 4 (top). The features displayed by this composition are similar to those of PZT with  $x=0.48$  [4]. A comparison with the latter data at low temperatures shows that the monoclinic angle,  $\beta$ , is larger for  $x=0.46$  than for  $x=0.48$ . With decreasing  $x$  (Ti content), the differences between  $a_m$  and  $b_m$  also increase, while the difference between  $a_m$  and  $c_m$  decreases, corresponding to the evolution to a rhombohedral phase in which " $a_m = b_m = c_m$ " [4]. The monoclinic phase is very well-defined at low temperatures, as shown by the pseudo-cubic  $(110)_{pc}$  reflections plotted at the bottom left of Fig 4. The evolution of  $\beta-90^\circ$  shows a transition to a tetragonal phase at  $T_{T-M} \simeq 450$  K, in agreement with the MPB of Jaffe *et al.*. However, the characteristic features of the tetragonal phase also appear well below this temperature, and there is a wide region of phase coexistence between the tetragonal and monoclinic phases, as shown in the central plot at the bottom of the figure. In this plot the peak positions for the pseudo-cubic  $(110)_{pc}$  reflections corresponding to the monoclinic and tetragonal phases are shown together with the experimental data. From the observed data, a reliable peak fitting analysis can be carried out and the lattice parameters determined for both phases in this region, as plotted as a function of temperature at the top of Fig. 4. The measurements on PZT with  $x=0.47$  show similar behavior, but with a narrower coexistence region ( $300 \text{ K} < T < 400 \text{ K}$ ). For this composition the evolution of the order parameter,  $\beta - 90^\circ$ , suggests a tetragonal-to-monoclinic phase transition at  $T_{T-M} \simeq 310$  K, very close to that observed for  $x=0.48$ , but the sample is not fully tetragonal until the temperature is larger than 400 K, corresponding to the MPB of Jaffe *et al.* for this composition.

### B. Tetragonal-rhombohedral phase transition

A similar analysis for PZT with  $x=0.45$  yields completely different results, as shown by the evolution of the

(200)<sub>pc</sub> reflection, in the lower part of Fig. 5. At low temperature the sample is rhombohedral (left) and remains rhombohedral up to  $T \simeq 500$  K, while for  $T > 550$  K, this composition is tetragonal. Some diffuse scattering is observed between the tetragonal peaks, as shown in the bottom right of Fig. 5. This feature is present in all compositions in the study, as previously noted in ref. [4], and is associated with the existence of twin boundaries in the tetragonal ferroelectric phase [33]. From the evolution of the order parameter ( $90^\circ - \alpha_r$ ), it is possible to determine that the tetragonal-rhombohedral phase transition is complete at  $T_{T-R} \simeq 580$  K. A coexistence region is observed in the interval  $500 \text{ K} < T < 580$  K. In the central plot at the bottom of the figure, the (200)<sub>pc</sub> reflection in this region is depicted, together with the calculated peak positions for both phases.

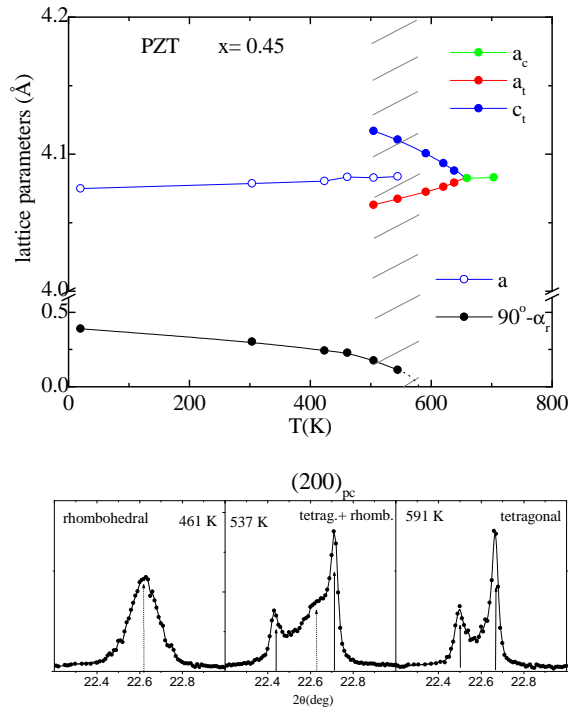


FIG. 5. Temperature evolution of the lattice parameters of PZT with  $x = 0.45$  from 20 K to 710 K, for the rhombohedral,  $a$  and  $\alpha_r$ ; tetragonal,  $a_t$  and  $c_t$ ; and cubic,  $a_c$ , phases. The dashed area in the figure represents the region of tetragonal and rhombohedral phase coexistence. At the bottom of the figure the pseudo-cubic (200) reflection is plotted at 461 K (rhombohedral phase), 537 K (tetragonal/rhombohedral phase coexistence) and 591 K (tetragonal phase), where the calculated peak positions are indicated by dashed arrows in the rhombohedral phase and solid arrows in the tetragonal phase.

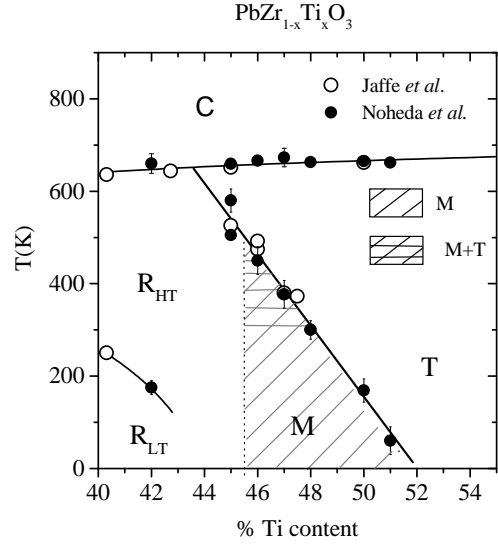


FIG. 6. New PZT phase diagram around the MPB. The solid symbols are the results from the current work, together with those in ref. 3 ( $x = 0.50$ ) and ref. 4 ( $x = 0.48$ ). Data from Jaffe *et al.* [1] and Amin *et al.* [36] are represented by open circles. The monoclinic region is shaded with diagonal lines. Horizontal lines are superimposed in the region of tetragonal-monoclinic phase coexistence. For  $x = 0.45$  the solid symbols represent the limits of the tetragonal-rhombohedral coexistence region.

### C. Low temperature rhombohedral phase

The data obtained for the PZT sample with  $x = 0.42$  show that this composition has rhombohedral symmetry all the way down to 20 K from the Curie point at  $T_c \simeq 650$  K. At 20 K the rhombohedral lattice parameters are  $a = 4.0921$  Å and  $\alpha_r = 89.61^\circ$ . With increasing temperature, the rhombohedral angle,  $\alpha_r$ , increases gradually until the cubic phase is reached, while  $a$  remains practically constant.

Two different rhombohedral phases have been observed in PZT: a high-temperature phase ( $F_{R(HT)}$ ) and a low temperature rhombohedral phase ( $F_{R(LT)}$ ) [34], which have space groups  $R3m$  and  $R3c$ , respectively. In the latter phase, adjacent oxygen octahedra along the [111] polar axis are rotated about this axis in opposite directions, so that the unit cell is doubled with respect to the high-temperature phase [35,36]. The corresponding phase boundary was also determined by Jaffe *et al.* [1] in the region of the phase diagram above room temperature. An extension of this boundary below room temper-

ature was reported in a neutron powder diffraction study by Amin et al. [37], who investigated the superlattice peaks from a sample with  $x=0.40$  and found the transition temperature to occur at about 250 K. In the present work, we were also able to observe very weak superlattice peaks from a composition with  $x=0.42$  below room temperature in the synchrotron x-ray patterns. The phase boundary in this case was found to lie at approximately 175 K (see fig. 6).

We have also observed one very weak superlattice peak in a recent neutron diffraction study of a sample with  $x=0.48$  at 20 K. This peak can be indexed in terms of a monoclinic cell with a doubled c-axis, but the nature of the distortion and any possible relationship with that in the low-temperature rhombohedral phase has not yet been determined.

#### IV. DISCUSSION

The results presented above are summarized and compared with previous data from  $x=0.48$  and  $x=0.50$  in Figure 6, which represents the new PZT phase diagram around the MPB. The data obtained for the tetragonal-(monoclinic/rhombohedral) transition temperatures for  $0.45 < x < 0.51$  are very consistent and lie on a well-defined line, which reproduces the MPB of Jaffe et al. [1] above ambient temperature. The boundary between the rhombohedral and monoclinic regions is shown as a vertical line between  $0.45 < x < 0.46$ , since no evidence of a monoclinic-rhombohedral phase transition has been observed. The lattice parameters at 20 and 300 K for the compositions under study are listed in Table 1, which also shows clearly the widening of the monoclinic region at lower temperatures. Figure 7 shows the evolution of the lattice parameters of the different phases as a function of composition at 300 K, from the rhombohedral to the tetragonal PZT phases via the monoclinic phase. At

the top of the figure, the unit cell volume shows an essentially linear behavior with composition in the range studied. The monoclinic angle,  $\beta$ , and lattice strain,  $c/a$ , at 300 K are also plotted as a function of composition in Fig. 7, where the rhombohedral cell with lattice parameters  $a$  and  $\alpha_r$  (see Table 1) has been expressed in terms of the monoclinic cell [38].  $c/a$  corresponds to  $c_t/a_t$ ,  $2\sqrt{2}c_m/(a_m + b_m)$  and 1, in the tetragonal, monoclinic and rhombohedral cases, respectively.  $\beta$  is  $90^\circ$  for a tetragonal cell and is the monoclinic angle for the monoclinic cell. The role of the monoclinic phase as a "bridge" between the tetragonal and rhombohedral phases in PZT is clearly demonstrated in these plots. The monoclinic phase has also been observed by Raman scattering in a very recent paper by Souza Filho et al. [39].

The structural studies reported here, together with those in refs. [2-4], comprise data from ten samples from two different origins spanning the composition range  $0.42 \leq x \leq 0.52$ . As mentioned earlier, only one of these samples was inconsistent with the picture shown in Fig. 6, namely PZT with  $x=0.47$  described in ref. [3]. For this composition it was found that the tetragonal phase transformed to a rhombohedral phase at low temperatures, while, at intermediate temperatures, a poorly-defined region of coexisting phases was observed. On the other hand, the data for the  $x=0.47$  sample studied in the present work shows, as described above, characteristics similar to those of  $x=0.46$  or  $x=0.48$ ; in particular, the existence of a monoclinic phase at low temperatures and no traces of a rhombohedral phase. It is noteworthy that an analysis of the peak-widths in the cubic phase shows clear differences in the microstructure of the two sets of samples. The microstrain,  $\Delta d/d$ , and crystallite-size of the samples used in the present study are estimated to be about  $3 \times 10^{-4}$  and  $1 \mu\text{m}$ , respectively [4]. A similar analysis for the  $x=0.47$  sample described in ref. [3] yields values of  $11 \times 10^{-4}$  and  $0.2 \mu\text{m}$ , respectively. One possible explanation is that because of the smaller crystallite size

TABLE I. Lattice parameters at 20 and 300K for PZT with  $x$  in the range 0.42-0.52. The symmetry, S, of the unit cell, rhombohedral(R), monoclinic (M) or tetragonal (T) is indicated in each case. For rhombohedral symmetry  $a = b = c$  and  $\alpha_r$  is the rhombohedral angle. In the monoclinic case,  $\beta$  is the monoclinic angle. In the tetragonal case  $a = b = a_t$  and  $\beta = 90^\circ$

% Ti	20 K						300 K					
	S	$a$ (Å)	$b$ (Å)	$c$ (Å)	$\alpha_r$ ( $^\circ$ )	$\beta$ ( $^\circ$ )	S	$a$ (Å)	$b$ (Å)	$c$ (Å)	$\alpha_r$ ( $^\circ$ )	$\beta$ ( $^\circ$ )
42	R	4.078			89.61		R	4.084			89.68	
45	R	4.075			89.61		R	4.079			89.69	
46	M	5.747	5.721	4.104		90.62	M	5.754	5.731	4.103		90.47
47	M	5.731	5.713	4.123		90.58	M	5.720	5.715	4.142		90.22
48	M	5.717	5.703	4.143		90.53	T	4.041		4.140		
50	M	5.693	5.690	4.159		90.35	T	4.032		4.147		
51	M	5.681	5.680	4.169		90.22	T	4.028		4.146		
52	T	4.009		4.158			T	4.030		4.145		



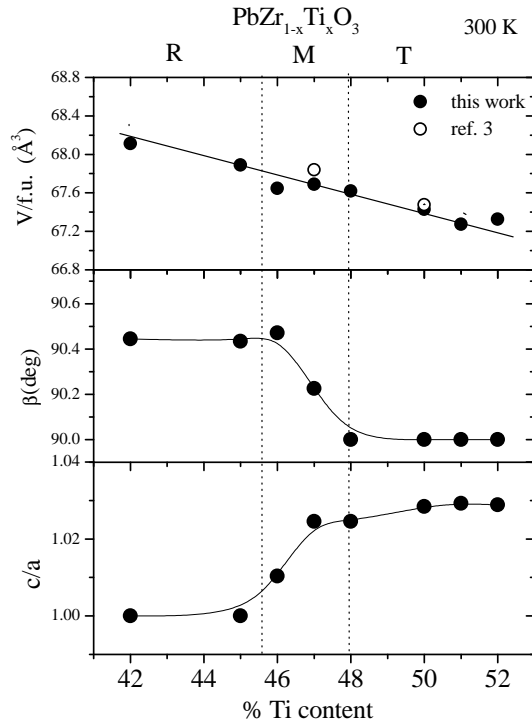


FIG. 7. The structural evolution with composition from the rhombohedral to the tetragonal PZT phases, through the monoclinic phase, as illustrated by the cell volume per formula unit,  $V$  (top), the monoclinic angle,  $\beta$  (center) [38], and the lattice strain,  $c/a$  (bottom) for PZT with  $0.42 \leq x \leq 0.52$  at 300 K. The cell volumes of the samples in ref.[3] are also plotted as open circles at the top of the figure.

in the ceramic samples in ref. [3], the inhomogeneous internal stress "prematurely" induces the tetragonal-rhombohedral phase transitions and inhibits the formation of the intermediate monoclinic phase. With a larger crystallite size, the internal strain is more easily relieved [40,41], presumably through the formation of non-180° domains [42], and the monoclinic phase transition is stabilized.

It is interesting to address the question of why the monoclinic phase was not observed in any of the previous studies. One important factor is the much superior resolution of synchrotron powder diffraction equipment compared to that of laboratory equipment; a second is the presence of wide regions of rhombohedral-tetragonal phase coexistence in many of these studies, due to compositional fluctuations and/or small grain sizes [8,43–46], which would obscure the evidence for monoclinic symmetry. For samples prepared by conventional "dry" solid-state techniques, a much narrower range of compositional fluctuations and large grain size can be achieved by the use of a final heat treatment at 1250 °C, as in the present case, or by the use of "semi-wet" methods of synthesis and lower firing temperatures [47–50]. However, perhaps the key element for clarifying the phase diagram is to

carry out the structural studies at low temperatures, as clearly demonstrated in Fig. 6.

Very recently, experiments on poled samples by Guo et al. [51] have further underlined the crucial role of the monoclinic phase in PZT. These experiments have revealed that poling induces the monoclinic distortion. The application of an electric field causes the rotation of the polar axis and an associated monoclinic distortion, which is retained after the field is removed. These features are shown to be the origin of the high piezoelectric response in PZT. It is observed that for rhombohedral PZT close to the MPB the region of stability of the monoclinic phase increases after an electric field is applied. The field-induced monoclinic phase is found to be considerably wider on the Zr side of the phase diagram, at room temperature, extending at least to a Ti content of  $x=0.42$ . These experiments [51] validate the microscopic model for the MPB proposed in ref. [4]; i.e. the application of a field would favor one of the local sites, which corresponds exactly to the observed monoclinic distortion (see the dashed arrow in the top-left plot of Fig. 1), and induces the monoclinic phase (see the top-right plot in Fig. 1). Further studies of the poled samples are in progress, and will be reported in a subsequent publication.

#### Acknowledgments

The authors are especially grateful to J.A. Gonzalo and S-E. Park, who were collaborators in the initial stages of this investigation, for their advice and encouragement. We also wish to thank L. Bellaiche, T. Egami, E. Salje, B.A Tuttle, D. Vanderbilt and T. Vogt for very helpful discussions. Financial support by the U.S. Department of Energy, Division of Materials Sciences (contract No. DE-AC02-98CH10886) and ONR (MURI project N00014-96-1-1173) is also acknowledged.

- [1] B. Jaffe, W.R. Cook, and H. Jaffe, *Piezoelectric Ceramics* (Academic Press, London, 1971).
- [2] B. Noheda, D.E. Cox, G. Shirane, J.A. Gonzalo, L.E. Cross, and S-E. Park, *Appl. Phys. Lett.* **74**, 2059 (1999).
- [3] B. Noheda, J.A. Gonzalo, A.C. Caballero, C. Moure, D.E. Cox, and G. Shirane, *Ferroelectrics* **237**, 237 (2000). e-print:cond-mat/9907286.
- [4] B. Noheda, J.A. Gonzalo, L.E. Cross, R. Guo, S-E. Park, D.E. Cox and G. Shirane, *Phys. Rev. B* **61**, 8687 (2000).
- [5] G. Shirane and K. Suzuki, *J. Phys. Soc. Japan* **7**, 333 (1952).
- [6] E. Sawaguchi, *J. Phys. Soc. Japan* **8**, 615 (1953).
- [7] L. Hanh, K. Uchino, and S. Nomura, *Jpn. J. Appl. Phys.* **17**, 637 (1978).
- [8] W. Cao and L.E. Cross, *Phys. Rev. B* **47**, 4825 (1993).
- [9] S.K. Mishra, D. Pandey, and A. Singh, *Appl. Phys. Lett.*

- 69**, 1707 (1996).
- [10] X-h Du, J. Zheng, U. Belegundu, and K. Uchino, Appl. Phys. Lett. **72**, 2421 (1998).
  - [11] S. Teslic, T. Egami, and D. Viehland, J. Phys. Chem. Solids **57**, 1537 (1996); Ferroelectrics **194**, 271 (1997).
  - [12] J. Ricote, D.L. Corker, R. W. Whatmore, S.A. Impey, A.M. Glazer, J. Dec, K. Roleder. J. Phys.:Condens. Matter **10**, 1767 (1998).
  - [13] D.L. Corker, A.M. Glazer, R.W. Whatmore, A. Stallard, and F. Fauth, J. Phys.:Condens. Matter **10**, 6251 (1998).
  - [14] R. E. Cohen, Nature (London) **358**, 136 (1992).
  - [15] R.D. King-Smith and D. Vanderbilt, Phys. Rev. B **49**, 5828 (1994).
  - [16] W. Zhong, D. Vanderbilt, and K. Rabe, Phys. Rev. Lett. **73**, 1861 (1994) and Phys. Rev. B **52**, 6301 (1995).
  - [17] A. Garcia and D. Vanderbilt, Phys. Rev. B **54**, 3817 (1996).
  - [18] A. Garcia and D. Vanderbilt, Appl. Phys. Lett. **72**, 2981 (1998).
  - [19] U.W. Waghmare and K.M. Rabe, Phys. Rev. B **55**, 6161 (1997).
  - [20] K. M. Rabe and E. Cockayne, *Proceedings of the AIP Conference A* **436**, 61 (1998). e-print: cond-mat/9804056
  - [21] Ph. Ghosez, E. Cokayne, U.V. Waghmare, and K.M. Rabe, Phys. Rev. B **60**, 836 (1999).
  - [22] L. Bellaiche, J. Padilla, and D. Vanderbilt, Phys. Rev. B **59**, 1834 (1999).
  - [23] G. Saghi-Szabo, R. E. Cohen, and H. Krakauer, Phys. Rev. B **59**, 12771 (1999).
  - [24] B.P. Burton and E. Cockayne, Phys. Rev. B **60**, R12542 (1999).
  - [25] H. Fu and R. Cohen, Nature **403**, 281 (2000).
  - [26] L. Bellaiche, and D. Vanderbilt, Phys. Rev. Lett. **83**, 1347 (1999)
  - [27] L. Bellaiche, A. Garcia, and D. Vanderbilt, Phys. Rev. Lett. **84**, 5427 (2000)
  - [28] L.W. Finger, D.E. Cox, and A.P. Jephcoat, J. Appl. Crystallogr. **27**, 892 (1994).
  - [29] A. M. Glazer and S. A. Mabud, Acta Cryst. B **34**, 1065 (1978).
  - [30] R. J. Nelmes and W.F. Kuhs, Solid State Commun. **54**, 721 (1985).
  - [31] G. Shirane, R. Pepinski, and B.C. Frazer, Acta Cryst. **9**, 131 (1956).
  - [32] G.A. Rosetti, Jr. and A. Navrotsky, J. of Solid State Chem. **144**, 188 (1999).
  - [33] A.I. Ustinov, J.-C. Niepce, C. Valot, L.A. Olikhovska, and F. Bernard, Mater. Science Forum **321-324**, 109 (2000).
  - [34] H.M. Barnett, J. Appl. Phys. **33**, 1606 (1962).
  - [35] C. Michel, J.-M. Moreau, G.D. Achenbach, R. Gerson, and W.J. James, Solid State Comm. **7**, 865 (1969).
  - [36] A. M. Glazer, S. A. Mabud, and R. Clarke, Acta Cryst. B **34**, 1060 (1978).
  - [37] A. Amin, R.E. Newnham. L.E. Cross, and D.E. Cox, J. Solid State Chem. **37**, 248 (1981).
  - [38] The rhombohedral unit cell with lattice parameters  $a$  and  $\alpha_r$ , can be expressed in terms of a monoclinic unit cell as follows:  $a_m = 2a \cos(\alpha_r/2)$ ,  $b_m = 2a \sin(\alpha_r/2)$ ,  $c_m = a$  and  $\beta = 180^\circ - \arccos[(1 - 2\sin^2(\alpha_r/2))/\cos(\alpha_r/2)]$ .
  - [39] A.G. Souza Filho, K.C.V. Lima, A.P. Ayala, I. Guedes, P.T.C. Freire, J. Mendes Filho, E.B. Araujo and J.A. Eiras, Phys. Rev. B **61**, 14283 (2000).
  - [40] W.R. Buessem, L.E. Cross, and A.K. Goswami, J. Am. Ceram. Soc. **49**, 33 (1966)
  - [41] further details: B. Tuttle and D.A. Payne, Ferroelectrics **37**, 603 (1981).
  - [42] R.W. Cahn, Adv. Phys. **3**, 363 (1954).
  - [43] P. Ari-Gur and L. Benguigui, J. Phys. D: Appl. Phys. **8**, 1856 (1975).
  - [44] J.C. Fernandes, D.A. Hall, M.R. Cockburn, and G.N. Greaves, Nucl. Instr. and Meth. in Phys. Res. B **97**, 137 (1995).
  - [45] A.P. Wilkinson, J. Xu, S. Pattanaik, and S.J.L. Billinge, Chem. Mater. **10**, 3611 (1998).
  - [46] E. R. Leite, M. Cerqueira, L. A. Perazoli, R. S. Nasar, and E. Longo, J. Am. Ceram. Soc. **79**, 1563 (1996).
  - [47] K. Kakegawa, J. Mohri, T. Takahashi, H. Yamamura, and S. Shirasaki, Solid State Comm. **24**, 769 (1977).
  - [48] K. Kakegawa, J. Mohri, S. Shirasaki, and K. Takahashi, J. Am. Ceram. Soc. **65**, 515 (1982).
  - [49] A.P. Singh, S.K. Mishra, D. Pandey, Ch.D. Prasad, and R. Lal, J. of Mat. Sci. **28**, 5050 (1993).
  - [50] A. Cüneyt Taş, J. Am. Ceram. Soc. **82**, 1582 (1999).
  - [51] R. Guo, L.E. Cross, S-E. Park, B. Noheda, D.E. Cox, and G. Shirane, Phys. Rev. Lett. **84**, 5423 (2000).